

Spatial assessment of landslide risk using two novel integrations of neuro-fuzzy system and metaheuristic approaches; Ardabil Province, Iran

Hossein Moayedı , Mahdy Khari , Mehdi Bahiraei , Loke Kok Foong & Dieu Tien Bui

To cite this article: Hossein Moayedı , Mahdy Khari , Mehdi Bahiraei , Loke Kok Foong & Dieu Tien Bui (2020) Spatial assessment of landslide risk using two novel integrations of neuro-fuzzy system and metaheuristic approaches; Ardabil Province, Iran, Geomatics, Natural Hazards and Risk, 11:1, 230-258, DOI: [10.1080/19475705.2020.1713234](https://doi.org/10.1080/19475705.2020.1713234)

To link to this article: <https://doi.org/10.1080/19475705.2020.1713234>



© 2020 The Author(s). Published by Informa UK, Limited trading as Taylor & Francis Group.



Published online: 29 Jan 2020.



[Submit your article to this journal](#)



Article views: 657



[View related articles](#)




[View Crossmark data](#)



Citing articles: 4 [View citing articles](#)



Spatial assessment of landslide risk using two novel integrations of neuro-fuzzy system and metaheuristic approaches; Ardabil Province, Iran

Hossein Moayed^a , Mahdy Khari^b, Mehdi Bahiraei^c, Loke Kok Foong^{d,e} and Dieu Tien Bui^f

^aInstitute of Research and Development, Duy Tan University, Da Nang, Vietnam; ^bDepartment of Civil Engineering, East Tehran Branch, Islamic Azad University, Tehran, Iran; ^cFaculty of Engineering, Razi University, Kermanshah, Iran; ^dDepartment for Management of Science and Technology Development, Ton Duc Thang University, Ho Chi Minh City, Vietnam; ^eFaculty of Civil Engineering, Ton Duc Thang University, Ho Chi Minh City, Vietnam; ^fDepartment of Business and IT, University of South-Eastern Norway, Bø i Telemark, Norway

ABSTRACT



This article addresses the spatial analysis of landslide susceptibility in the Ardabil province of Iran. To this end, two well-known optimization algorithms, namely genetic algorithm (GA) and particle swarm optimization (PSO) are synthesized with an adaptive neuro-fuzzy inference system (ANFIS) to create the ensembles of GA-ANFIS and PSO-ANFIS. Besides, the statistical index (SI) model is also performed to be compared with the mentioned intelligent techniques. Fourteen landslide conditioning factors including elevation, slope aspect, land use, plan curvature, profile curvature, soil type, distance to river, distance to road, distance to fault, rainfall, slope degree, stream power index (SPI), topographic wetness index (TWI), and lithology were considered within the geographic information system (GIS). Out of 253 identified landslides, 177 points (70% of them) were randomly selected and used for the training phase, and the remaining 76 points (30% of them) were used to evaluate the accuracy of the SI, GA-ANFIS, and PSO-ANFIS models. Referring to the calculated area under the receiver operating characteristic curve (AUROC) index, the GA-ANFIS (AUROC = 0.914) and SI (AUROC = 0.821) showed the best performance, respectively in the training and testing phases. Notably, ANFIS-PSO emerged as the faster prediction method compared to the GA-ANFIS. Also, from spatial analysis, it was revealed that around 95%, 87%, and 97% of the training landslides, and 96%, 84%, and 76% of the testing landslides are located in hazardous areas.

ARTICLE HISTORY

Received 6 May 2019
Accepted 6 January 2020

KEYWORDS

Landslide susceptibility mapping; ANFIS; particle swarm optimization; genetic algorithm

CONTACT Loke Kok Foong  lokokfoong@tdtu.edu.vn  Department for Management of Science and Technology Development, Ton Duc Thang University, Ho Chi Minh City, Vietnam; Faculty of Civil Engineering, Ton Duc Thang University, Ho Chi Minh City, Vietnam

© 2020 The Author(s). Published by Informa UK, Limited trading as Taylor & Francis Group.

This is an Open Access article distributed under the terms of the Creative Commons Attribution License (<http://creativecommons.org/licenses/by/4.0/>), which permits unrestricted use, distribution, and reproduction in any medium, provided the original work is properly cited.

1. Introduction

As a ubiquitous disaster, slope failures cause plenty of financial and psychological damages all over the world every year. According to Varnes and Radbruch-Hall (1976), the landslide is defined as all kinds of gravity-caused downward mass movements on slopes. Artificial deposits, soil, and natural cliffs are examples of these masses than landslide can occur over them. According to global reports, more than 90% of the occurred landslides have been located in developing countries. Besides, landslides cause and at least 17% of the reported fatalities worldwide (Pourghasemi, Mohammady, et al. 2012). Iran is considered as a landslide-prone country due to many landslides occurred in recent years. It also has witnessed the most massive debris flow in the World (Seimareh landslide) (Shoaei and Ghayoumian 1998). Furthermore, according to the Iranian Landslide Working Party, landslides are responsible for about 187 losses of lives in Iran (Pourghasemi, Pradhan, et al. 2012).

For the purpose of decreasing these damages, evaluation of the landslide susceptibility of an area can be effective (Hong et al. 2019). Landslide susceptibility may be introduced as the spatial possibility of the landslide events based on a collection of geological and environmental situations. In this regard, various techniques in the field of landslide susceptibility mapping can be used for different landslide-prone areas worldwide (Chen et al. 2018; Kornejady and Pourghasemi 2019). Therefore, many researchers concerned the development of landslide susceptibility maps along with extracting relations for predicting the landslide susceptibility index in order to explore the landslide occurrence likelihood (Vakhshoori and Zare 2016; Kaur et al. 2019). They commonly perform the required approximation by the assist of a spatial dataset including different landslide conditioning parameters such as type of soil, slope, altitude, aspect, rainfall, lithology, climate, distance for linear phenomena (e.g. roads and drainage lines), stream power index (SPI), faults, etc. In addition, other researchers considerably addressed landslide risk evaluation by selecting simple predictive approaches such as the index of entropy (IOE), frequency ratio (FR), statistical index (SI), regression-based methods, and certainty factor (CF) (Demir et al. 2015; Youssef et al. 2015; Gao, Wang, et al. 2018; Gao, Wu, et al. 2018; Gao et al. 2019). The performance of a spatial logistic regression (SLR) approach in the case of landslide susceptibility modeling in a specific case study (Duwen Highway Basin at Sichuan Province located in China) was investigated by Yang et al. (2019). In addition, in order to the proper selection of the landslide-related parameters, they developed a GeoDetector-based method. The estimation precision of their suggested model was about 11.9% improved in comparison to the ordinary logistic regression (LR) model. Wang et al. (2015) utilized IOE together with certainty factor (CF) approaches to evaluate the landslide occurrence risk of Qianyang County located in China using fifteen landslide conditioning parameters of the geomorphology, topographic wetness index (TWI), slope aspect, slope angle, general curvature, rainfall, lithology, plan curvature, profile curvature, distance to faults, distance to rivers, distance to roads, altitude, sediment transport index, and SPI. Finally, CF yielded the landslide susceptibility map with higher reliability compared to IOE, according to the respective precisions of 82.32% and 80.88%.

Recently, soft computing (SC) methods (Zhoug et al., 2020, Weibiao, 2019) are widely used for establishing a fast, efficient, and inexpensive estimation of engineering parameters (Polykretis et al. 2017; Gao, Dimitrov, et al. 2018; Gao, Guirao, et al. 2018; Chen, Yan, et al. 2019) as well as other landslide susceptibility (Azad et al. 2019; Malik et al. 2019; Qiao and Yang 2019b; Qiao, Yang, et al. 2020; Qiao and Yang 2020). In this way, Oh and Pradhan (2011) selected an adaptive neuro-fuzzy inference system (ANFIS) designed with four membership functions (MF), namely trapezoidal, triangular, polynomial, and generalized bell. They concluded that ANFIS might operate as a promising approach in the territorial estimation of landslide susceptibility mapping. Lee et al. (2017) conducted a support vector machine (SVM) in the case of evaluation of landslide susceptibility for Pyeong Chang and Inje areas located in Korea and determined that the suggested SVM is a reliable tool for the mentioned purpose regarding the obtained precisions of 81.36% and 77.49%, respectively for the PyeongChang and Inje zones. In addition, many scholars have conducted a comparison among various landslide evaluative approaches. He et al. (2019) have compared the performance of radial basis function (RBF), Naïve Bayes (NB), Classifier, and RBF neural for estimating the landslide susceptibility zonation in Longhai zone located in China. It is noteworthy that they employed FR and SVM for calculating the effectiveness of each landslide conditioning parameter and found that the RBF classifier has higher accuracy by 88.1% better than NB and RBF Network with respective accuracies of 87.2% and 0.85.4%. Moreover, Chen, Pourghasemi, et al. (2017) evaluated the performance of three novel predictive models, including ANFIS-FR (ANFIS synthesized with FR), SVM, and generalized additive model (GAM) in landslide probability assessment at Hanyuan County located in China. This work showed the superiority of the SVM compared to ANFIS-FR and GAM, with obtained accuracies of 87.5%, 85.1%, and 84.6%, respectively. Also, Bagheri et al. (2018) mapped the seismic rockfall of the Firooz Abad-Kojour earthquake (occurred in 2004) by using LR and ANFIS predictive tools. Referring to the obtained results, ANFIS outperformed LR.

Numerous hybrid algorithms are introduced to have a more reliable prediction for most engineering complex problems (Fan et al. 2019; Liu et al. 2020; Qiao, Huang, et al. 2019; Zhang et al. 2019; Qiao and Yang 2019a; Chen et al. 2020; Qiao, Lu, et al. 2020). Furthermore, in order to enhance the performance of usual approaches such as ANN and ANFIS in diverse fields (e.g. landslide susceptibility mapping (Nguyen, Mehrabi, et al. 2019; Pham, Prakash, et al. 2019; Xi et al. 2019), groundwater quality modeling (Kisi et al. 2017), and also flood susceptibility mapping (Ahmadlou et al. 2018; Hong et al. 2018), different hybrid evolutionary methods have been widely designed and utilized by scholars. In this regards, Pham, Prakash, et al. (2019) used hybrid technique of Reduced Error Pruning Trees (REPT) to develop the ensembles of MultiBoost based Reduced Error Pruning Trees (MBREPT), Bagging based Reduced Error Pruning Trees (BREPT), Random Subspace-based Reduced Error Pruning Trees (RSREPT), and Rotation Forest-based Reduced Error Pruning Trees (RFREPT) for landslide susceptibility assessment. The findings of this research revealed the superiority of the BREPT method. Also, Moayedi et al. (2018) coupled an MLP neural network with particle swarm optimization (PSO) in the case of spatial

landslide susceptibility modeling at Kermanshah province, western Iran. They concluded that using PSO can facilitate obtaining more precise outputs. Nguyen et al. (2019c) conducted a case study for the combination of ANFIS and PSO (PS, O-ANFIS), Best First Decision Trees based Rotation Forest (RFBFDT), and the combination of ANN with PSO (PSO-ANN) for spatial landslide risk estimation in Vietnam. The computed Mean Square Error (MSE), Root Mean Square Error (RMSE) and the area under the curve (AUC) indicated the more robustness of the RFBFDT algorithm. Chen, Panahi, et al. (2017) also studied the robustness of PSO differential evolution (DE) and genetic algorithm (GA) techniques to enhance the ANFIS efficiency. Their results showed that the ANFIS-DE method outperformed ANFIS-GA, and ANFIS-PSO with respect to the calculated AUCs of 0.844, 0.821, and 0.780, respectively. Similarly, Tien Bui et al. (2016) optimized the least-squares support vector machines (LSSVM) model by utilizing the differential evolution (DE) technique in the case of rainfall-triggered landslide risk evaluation. They found that the suggested LSSVM model showed an accuracy of 82% accomplished more efficiently compared to other predictive methods (MLP, J48, and SVM algorithms). The computational deficiencies (e.g. local minima (Akkurt et al. 2003; Qiao, Tian, et al. 2019; Qiao and Yang 2019c) and dimension dangers (Chen, Panahi, et al. 2017)) associated with conventional intelligent models have driven the engineers to employ metaheuristic algorithms to remedy them. Two well-tried notions of these techniques are GA and PSO, which have shown high efficiency in earlier researches for optimizing predictor models. In this study, they are coupled with ANFIS for spatial estimation of landslide susceptibility at Ardabil province, Iran. Meanwhile, the main reason for selecting this area lies in the lack of attention despite the high occurred landslides over it. So, to fulfill this purpose, PSO-ANFIS, and GA-ANFIS, as well as a well-known statistical method (SI), are employed for proper mapping of landslide susceptibility in Ardabil province.

2. Study area

The study area is Ardabil Province, which is one of the northernmost regions of Iran. The exact location of Ardabil is shown in Figure 1. The city is roughly 17800 km^2 and lies within the longitude $47^{\circ}20'$ to $48^{\circ}60'$ E and latitude $37^{\circ}10'$ to $39^{\circ}40'$ N, west of the Caspian Sea. The altitude varies from 4 to 4785, and the majority of the area has a height between 2000 and 3000 meters above the sea level. Ardabil is known as one of the coldest regions of Iran with bitter winters and desirable weather during the summer. With an average annual rainfall of 316 millimeters and an average yearly temperature of 10.9°C , the presence of Sabalan mountains plays a significant role in air moderation of this region. The slope ranges between 0° and 63° , where the steep slopes (i.e. slope more than 45°) are rarely observed. According to the lithology map, Ardabil lies on diverse types of rocks (i.e. 25 lithology units), mainly two groups with the names “Andesitic volcanic” and “low-level piedment fan and valley terrace deposits.”

Figure 1 illustrates the location of the identified landslides and the considered non-landslide points. According to this map, the main concentration of the marked landslides is in the southern part of the Ardabil along with territorial roads and faults.

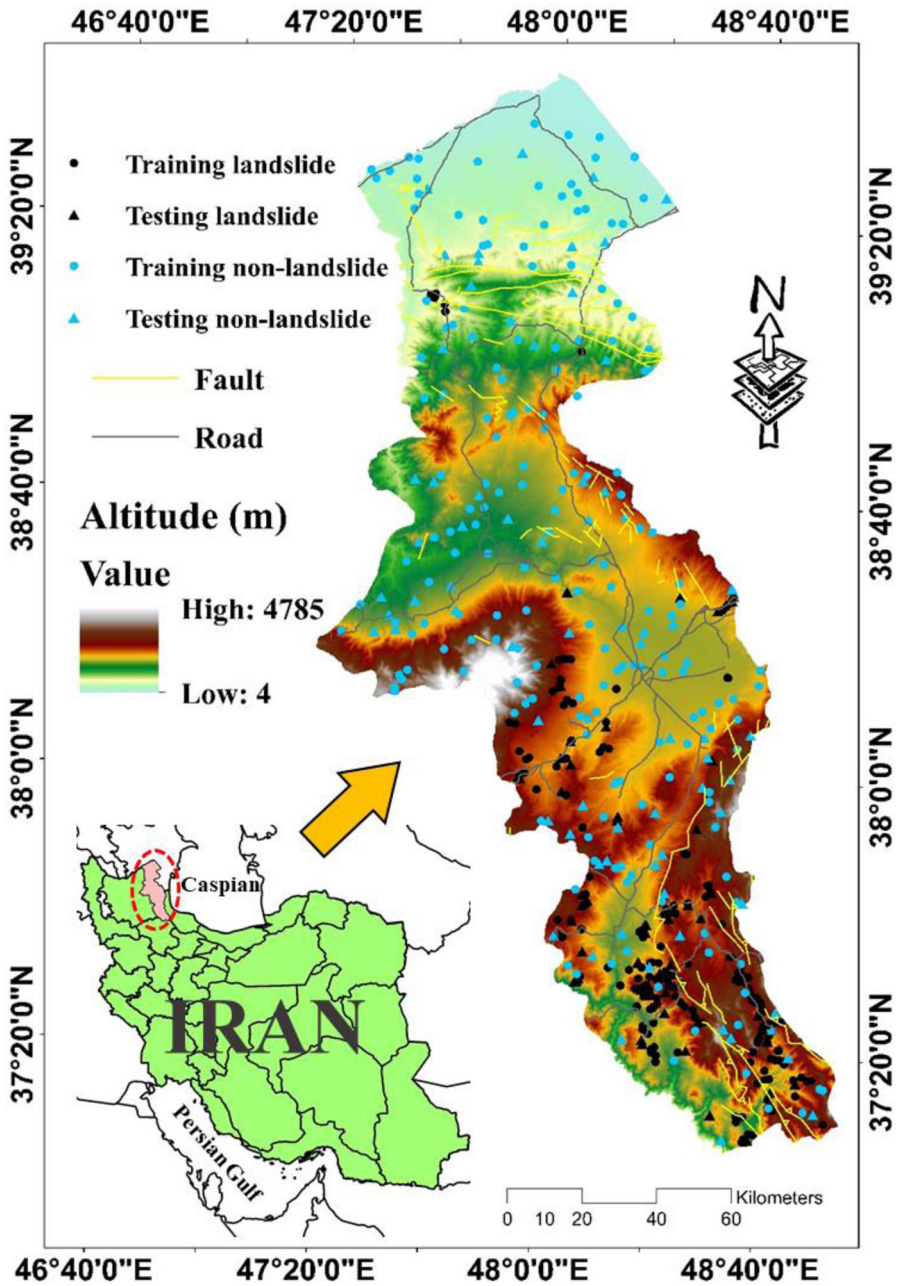


Figure 1. Location of the study area and spatial distribution of the landslides. Source: Author

3. Data preparation and spatial interaction between the landslide and conditioning parameters

Needless to say, providing a reliable spatial database is a crucial step in landslide susceptibility assessment. In this sense, the landslide inventory map, which plays the role of the response variable in intelligent models and interactive factors in statistical methods, is a significant parameter (Ercanoglu and Gokceoglu 2004). In this study,

utilizing the previous recorded, interpreting the aerial photos, and field monitoring (i.e. using GPS in 1:25000 scale), a total of 253 landslide points were identified within the Ardabil province. Out of those, 177 events (70% of the marked landslide points) were randomly selected and specified to train the proposed models, and the remaining 76 events (30% of the marked landslide points) were put aside for validating their performance. Then, 253 non-landslide points were also randomly produced within the places without any observed landslides. The same proportion was considered to divide the non-landslide points into the training and testing data (see [Figure 1](#)).

Fourteen of geological and hydrological landslide conditioning factors namely, elevation, slope aspect, land use, plan curvature, profile curvature, soil type, distance to river, distance to road, distance to fault, rainfall, slope degree, stream power index, topographic wetness index, and lithology were considered within the geographic information system (GIS). Note that all of the mentioned landslide-related factors were converted to raster format from their basic forms such as polygons, contours, polylines, etc. [Figure 2](#) denotes the area occupied by each sub-class in each landslide conditioning map, along with the calculated value of frequency ratio (FR). Assuming P_{ls} and P_{domain} as the percentage of the landslides located in the proposed sub-class and the percentage of the domain covered by it, respectively, then Equation (1) expresses the FR:

$$FR = \frac{P_{ls}}{P_{domain}} \quad (1)$$

Remarkably, the correlation between the landslide and the proposed sub-class is directly proportional to the FR value (Oh et al. 2011).

First, the digital elevation model (DEM) of the Ardabil was provided through landslide 8 imagery. Due to the proximity to the Caspian Sea, the lowest altitude of this area is close to the sea level (approximately 4 meters in the northern Ardabil), and it reaches more than 4700 meters in some districts. More than 30% of the area has an altitude in the range of [1056–1535] meters ([Figure 2\(a\)](#)). The obtained FRs of 2.34 and 1.26, respectively, for the altitude ranges of [1535–2003] and [2003–2664] show the high importance of these areas. The slope aspect map was derived from DEM layer and classified as: North (0–22.5°), North-East (22.5–67.5°), East (67.5–112.5°), South-East (112.5–157.5°), South (157.5–202.5°), South-West (202.5–247.5°), West (247.5–292.5°), North-West (292.5–337.5°) and North (337.5–360°). As [Figure 2 - \(d\)](#) denotes, the calculated FRs for the West, South-West, South, South-East, and East are above 1. Around three-fourth of the area is equally (i.e. 25%) classified as pasture, dry farming agriculture, and mountainous pastures. Analysis of the FR between the landslides and different utilization of lands demonstrate 2.51 and 1.37 values for the pasture and Oak forests, respectively. The influential factors of plan curvature and profile curvature are also derived from the DEM. 51% and 42% of the study area is labeled as convex (FR = 1.02) and concave (FR = 1.01) lands. As for profile curvature, the produced map is classified in three groups of (–2.76 to –0.001), (–0.001 to +0.001), and (0.001–5.17), with respective FRs of 0.97, 0.00, and 1.03. About the soil map, although, more than 40% of the area is covered by “Inceptisols” soil, the highest FR is obtained for “Mollisols” category (i.e. FR = 4.26 and percentage of the

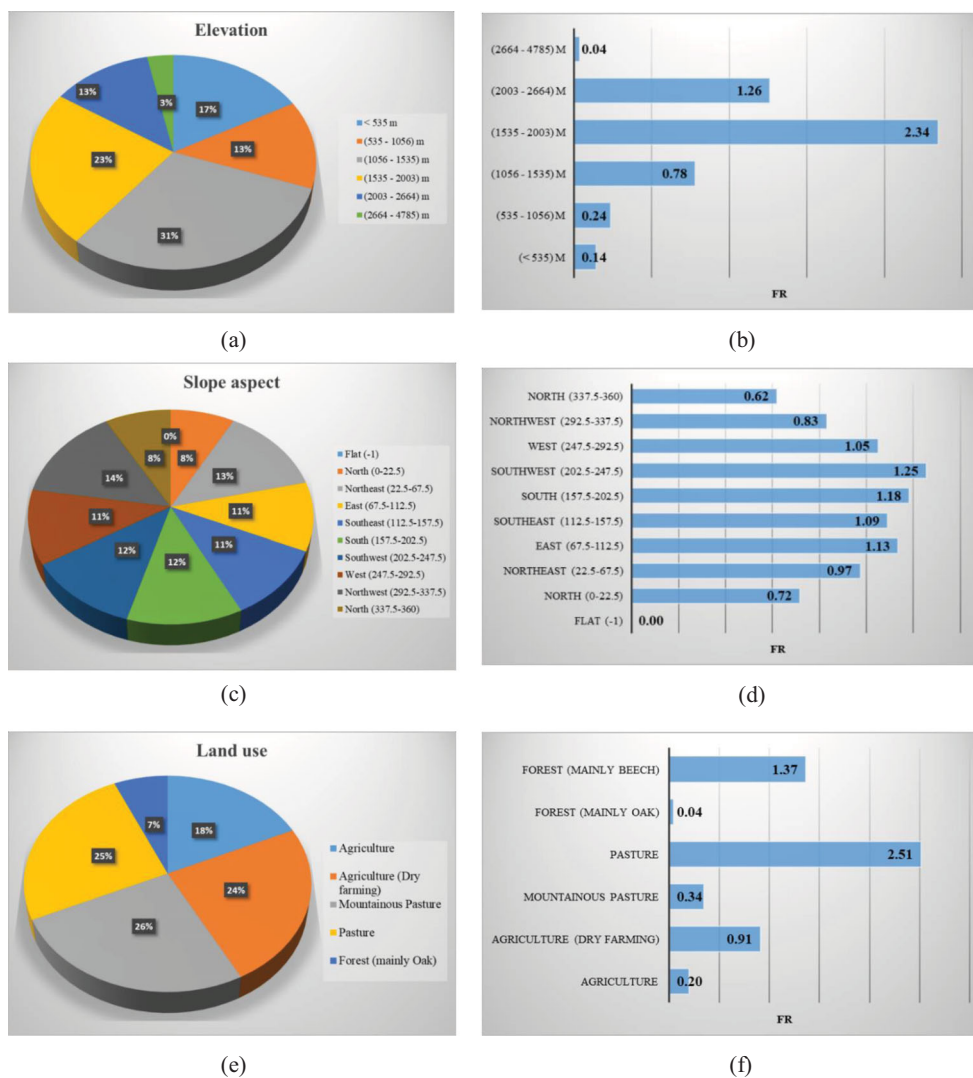
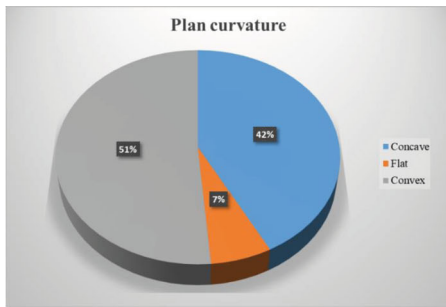


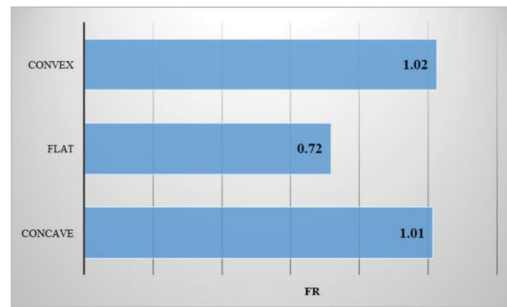
Figure 2. The percentage of the area for the sub-classes and the calculated FR for: (a and b) elevation, (c and d) slope aspect, (e and f) land use, (g and h) plan curvature, (i and j) profile curvature, (k and l) soil type, (m and n) distance to river, (o and p) distance from road, (q and r) distance from fault, (s and t) rainfall, (u and v) slope degree, (w and x) SPI, and (y and z) TWI landslide independent factors.

area = 2%) which shows the high landslide susceptibility of this group. Besides, three soil groups with the names “Aridisols,” “Rock Outcrops/Entisols,” and “Rock Outcrops/Inceptisols” gained considerable FRs.

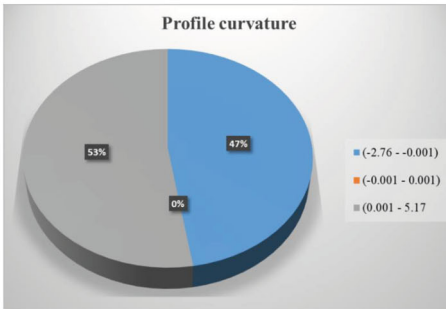
Moreover, to explore the effect of linear phenomena (i.e. the rivers, roads, and faults), three landslide independent factors of distance to rivers, and distance to roads, and distance to faults are considered. According to Figures 2 – (m), (o), and (q), these distances are classified into five sub-classes. For distance to the river, except the places farther than 700 meters, the other four groups gained the FR more than 1.10.



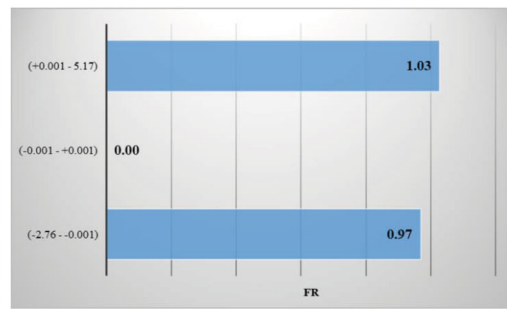
(g)



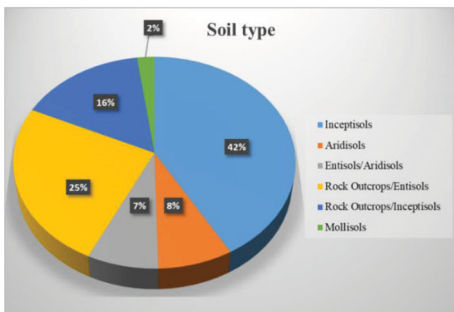
(h)



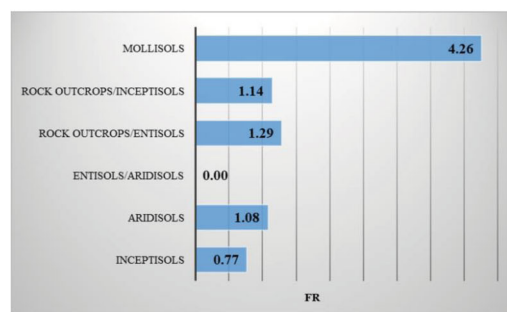
(i)



(j)



(k)



(l)

Figure 2. (Continued)

As for distance to road, the highest FR obtained for the distances between (0–100) meters (FR = 2.05), (100–300) meters (FR = 2.03), and (300–600) meters (FR = 1.95). Surprisingly about the distance to fault, the last distance group indicating the places further than 1200, gained the highest FR (i.e. 1.03). This is a while, and it is expected that the less distance to faults, the higher the impact on the occurrence of the landslide. The rainfall map was classified into five sub-classes. As expected, a higher FR has resulted as the value of the rainfall increases. Accordingly, the largest FR is 2.45 is observed for the rainfall sub-class of (519–815) millimeters. The slope layer was deduced from the DEM of Ardabil, and according to this map, half of the area contains slight slopes (lower than 5°). Notably, the steep slopes (i.e. more than 35°) are seldom observed. The largest FR values are 1.81 and 1.59, which are obtained for slope groups of (10–20)° and (20–35)°, respectively. Besides, to consider the impact of the geo-morphometric conditions, two well-known secondary factors of

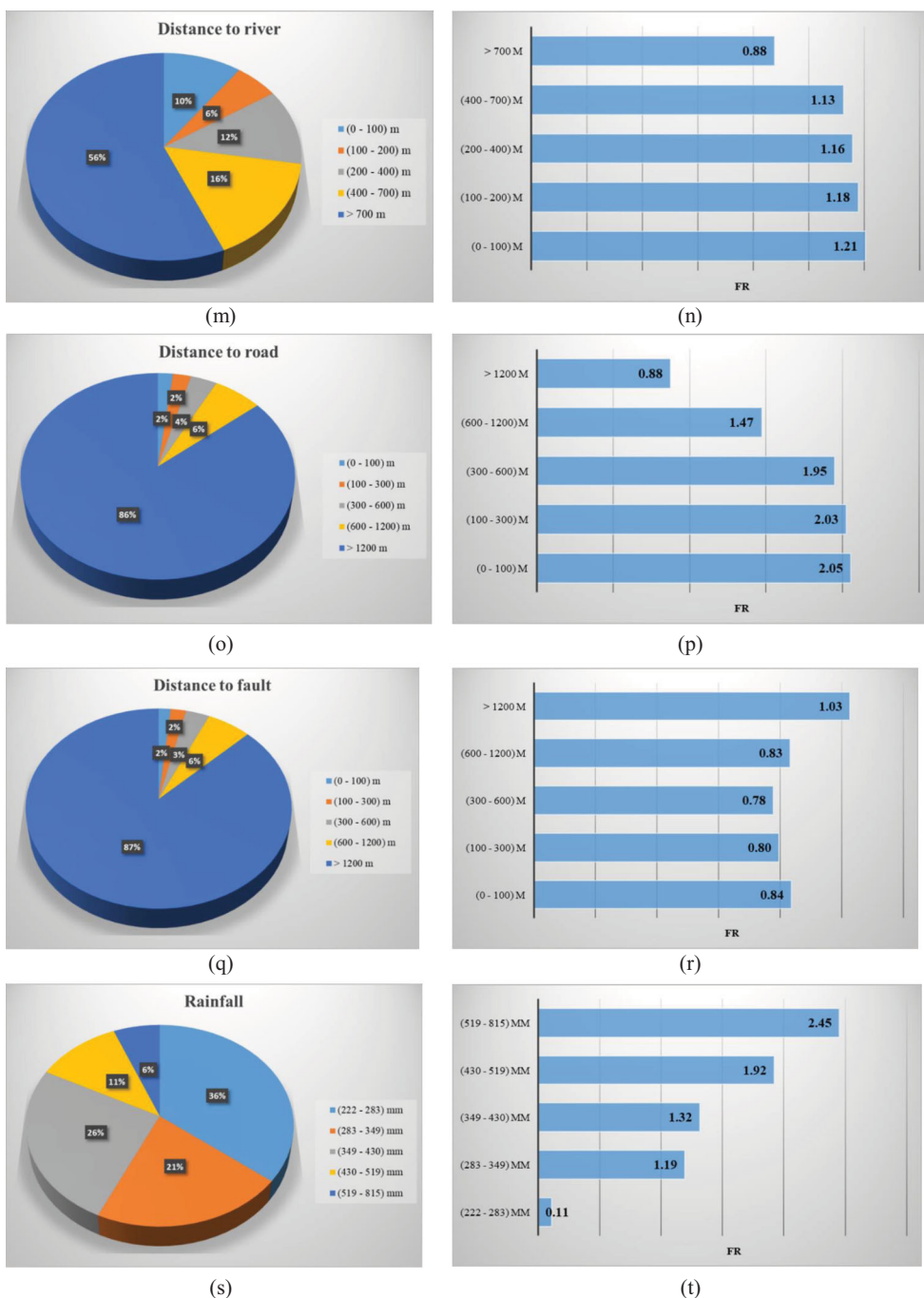
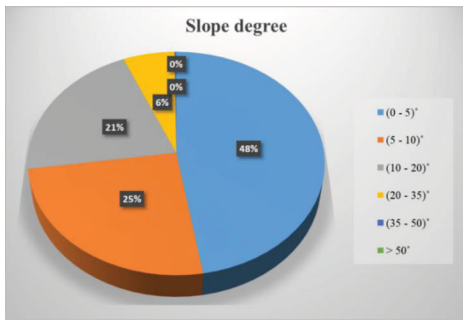
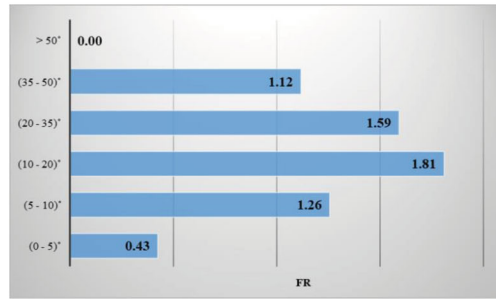


Figure 2. (Continued)

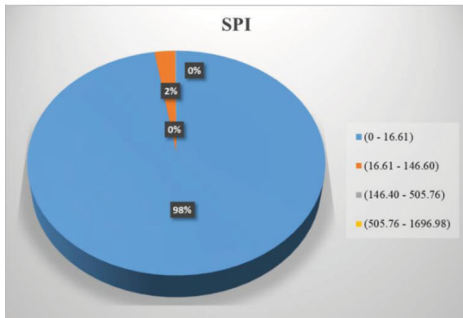
stream power index and topographic wetness index were developed, indicating the erosion power of streams and the amount of accumulated water in a place, respectively. Let α and β be the specific catchment and gradient, respectively, then Equations (2) and (3) denote the formulation of the SPI and TWI (Moore et al. 1991):



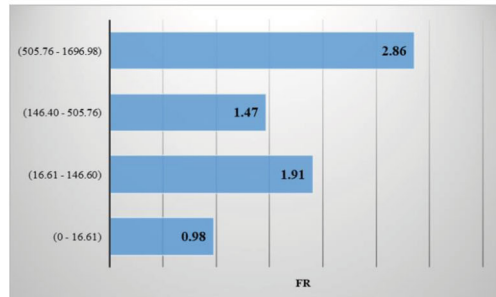
(u)



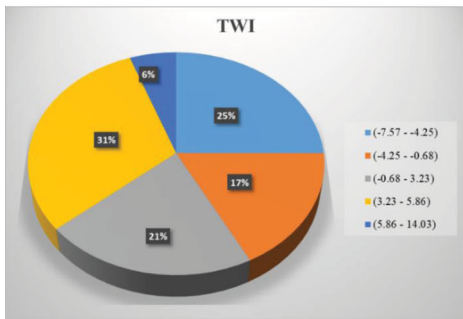
(v)



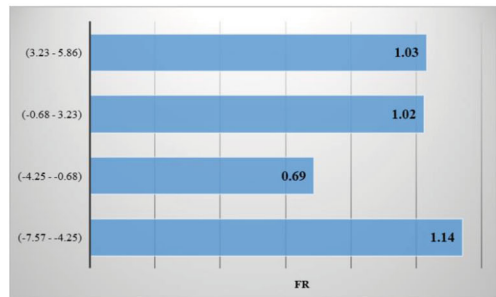
(w)



(x)



(y)



(z)

Figure 2. (Continued)

$$SPI = \alpha \times \tan \beta \quad (2)$$

$$TWI = \ln(\alpha / \tan \beta) \quad (3)$$

The highest calculated FRs were 2.86 and 1.14, which emerged for the largest and lowest extents of the SPI and TWI landslide causative factors, respectively. As explained before, the geology map of the study area is composed of 52 different lithology units, which are described in Table 1. According to this table, the most considerable FRs are obtained for the lithology categorizes of “Dark grey shale and sandstone (SHEMSHAK FM)” (FR = 7.50) and “Fluvial conglomerate, Piedmont conglomerate, and sandstone” (FR = 5.82).

Table 1. Description of the lithological units.

Lithology unit	Description	Percentage of the area	FR	Lithology unit	Description	Percentage of the area	FR
1	Stream channel, braided channel and flood plain deposits	0.76	0.00	27	Coarse-grained fanglomerate composed of volcaniclastic materials locally with intercalation of lava flows (Lahar)	4.61	1.14
2	High level piedmont fan and vally terrace deposits	11.94	0.24	28	Gypsiferous marl	0.01	0.00
3	Low level piedmont fan and vally terrace deposits	13.11	0.35	29	Andesitic tuff	0.01	0.00
4	Silty clay, sandy tuff and freshwater limestone (BakuFm)	2.30	0.00	30	Light grey, thin-bedded to massive limestone (LAR Fm)	0.44	4.39
5	Silty clay, sand, gravel and volcanic ash (Absheran Fm)	0.19	0.00	31	Conglomerate and sandstone	0.11	0.00
6	Varigated gypsiferous clay shale; conglomerate and sandstone	1.04	0.00	32	Pliocene andesitic subvolcanics	0.16	0.00
7	Polymictic conglomerate and sandstone	0.68	1.54	33	Dark grey shale and sandstone (SHEMSHAK Fm.)	1.52	7.50
8	Alternation of varigated siltyclay shale with sandstone	3.36	0.49	34	Dolomite and sandstone (Bayandour Fm)	0.05	0.05
9	Red marl, gypsiferous marl, sandstone and conglomerate (Upper red Fm.)	0.44	1.38	35	Granite to diorite	0.75	0.00
10	Massive to thick bedded tuffaceous sandstone and varigated shale	2.28	0.32	36	Rhyolitic to rhyodacitic tuff	0.88	0.00
11	Alternation of sandstone with siltstone and claystone	1.91	0.50	37	Andesite to basaltic volcanics	3.70	0.65
12	Alternations of marl, silty clay shale, sandstone and dolomitic limestone	0.36	1.34	38	Andesitic subvolcanic	0.50	0.00
13	Red Beds composed of red conglomerate, sandstone, marl, gypsiferous marl and gypsum	0.44	0.00	39	Rhyolitic to rhyodacitic volcanic tuff	0.13	0.00
14	Silty shale, marl, thin-bedded limestone, tuffaceous sandstone and basaltic volcanic rocks	0.04	0.00	40	Teravertine	0.21	0.85
15	Basal conglomerate and sandstone	0.70	0.00	41	Dacitic to andesitic subvolcanic rocks	4.31	2.31
16	Silty shale, marl, thin-bedded limestone, tuffaceous sandstone and basaltic volcanic rocks	0.70	0.00	42	Marl, shale, sandstone and conglomerate	4.36	1.77
17	Basaltic volcanic rocks	3.32	0.23	43	Andesitic and basaltic volcanics	0.07	0.00
18	Silty shale, sandstone, marl, sandy limestone, limestone and conglomerate	1.06	0.00	44	Marl, calcareous sandstone, sandy limestone and minor conglomerate	1.51	2.70

(continued)

Table 1. Continued.

Lithology unit	Description	Percentage of the area	FR	Lithology unit	Description	Percentage of the area	FR
19	Flysch turbidite, sandstone and calcareous mudstone	0.80	0.00	45	sandy to silty glauconitic limestone and calcareous limestone (Shal Fm)	0.69	0.68
20	Basaltic volcanic	0.18	0.00	46	Fluvial conglomerate, Piedmont conglomerate and sandstone.	0.83	5.82
21	Andesitic volcanic	4.14	0.00	47	Red and green silty, gypsiferous marl, sandstone and gypsum (Lower Red FM)	0.08	3.04
22	Low - grade, regional metamorphic rocks (Green Schist Facies)	0.07	0.00	48	Cretaceous rocks ingeneral	0.31	0.82
23	Andesitic volcanics	21.36	1.41	49	Dacitic to andesitic volcanic	0.73	5.36
24	Dacitic to Andesitic tuff	0.44	0.00	50	Gneiss, anatectic granite, amphibolite, kyanite, staurolite schist, quartzite and minor marble (Barreh Koshan Complex and Rutchan Complex)	0.82	1.85
25	Upper cretaceous, undifferentiated rocks	0.61	0.00	51	Andesitic basaltic volcanic	0.12	5.09
26	Andesitic volcanic tuff	0.52	0.00	52	Massive grey to black limestone	0.37	3.58

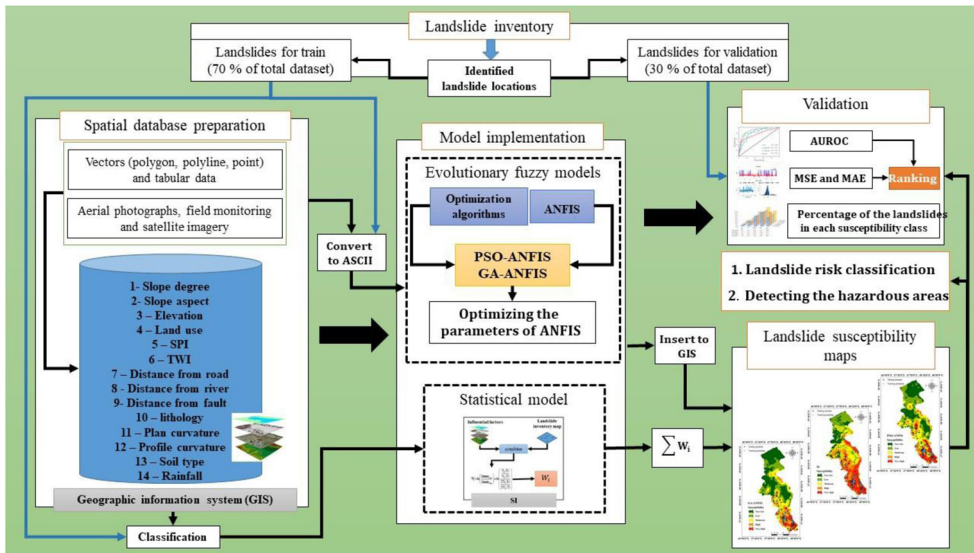


Figure 3. Graphical methodology of applied procedure for landslide susceptibility zonation.

4. Methodology

Figure 3 illustrates the overall process was carried out to produce the landslide susceptibility map of the study area. After providing the require GIS layers, all were converted to raster with 10×10 cell size. First, the existing landslide points were randomly divided into the training and testing sets. Then, the required dataset for developing the intelligent models were extracted through converting to ASCII format. In the following, by classifying the landslide independent factors, the spatial interaction between them and the training landslides were analyzed to perform the SI model. As for the ANFIS ensembles, the GA and PSO optimization algorithms were coupled with it, and after determining the optimal structures of them, the landslide susceptibility values were produced, and the maps were generated in the GIS environment. Finally, the accuracy of the produced landslide susceptibility maps was evaluated by the area under the receiver operating characteristic curve (AUROC) index.

The description of the used models is presented here:

4.1. Statistical index (SI) method

As a bivariate-based statistical method, the analytical index (SI) was first suggested by van Westen (van Westen 1997b) for a simple analysis of landslide susceptibility. The easiness of implementation can be mentioned as a merit of this model (Yesilnacar 2005). Different GIS options (e.g. data-driven analytical ability) can appropriately handle the SI method (Pourghasemi et al. 2013). The basis of this model is calculating a specific weight for each categorical unit of a landslide conditioning factor. It reveals the spatial interaction between the landslide points with the proposed independent factor. More clearly, the SI considers the frequency of the landslides for each sub-class of an independent factor and uses Eq. 4 to calculate the weight of the proposed sub-class (Cevik and Topal 2003):

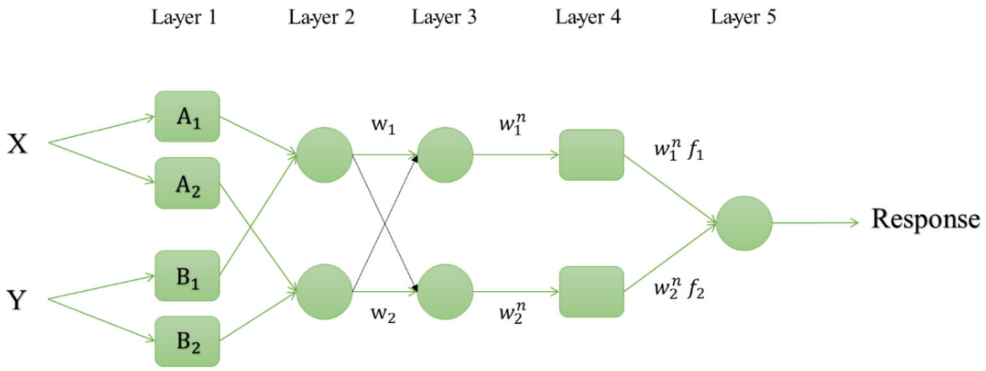


Figure 4. Typical ANFIS structure.

$$W_{SC} = \ln \left(\frac{D_{class}}{D_{map}} \right) = \ln \left(\frac{\frac{N_{pix}(D_i)}{N_{pix}(E_i)}}{\sum \frac{N_{pix}(D_i)}{N_{pix}(E_i)}} \right) \tag{4}$$

in which D_{class} and D_{map} denote the landslide density for the proposed sub-class and the studied area, respectively. The terms $N_{pix}(D_i)$ and $N_{pix}(E_i)$ stand for the number of prone cells and all cells, respectively.

This is noteworthy that although the outcome map of this model can be depicted with any extent of landslide susceptibility values, the main reason for employing natural logarithm lies in producing the positive and negative weights for comparing with the common situation (Van Westen 1997a).

4.2. An adaptive neuro-fuzzy inference system

Up to now, various artificial intelligence techniques have been developed for classifying and predicting many engineering problems through extracting the complicated mathematical relationship between the independent and response variables. Support vector machine (SVM), adaptive neuro-fuzzy inference system (ANFIS), and artificial neural networks (ANN) are well-known predictive methods. The name ANFIS implies a combination of fuzzy and neural learning theories. This model was first presented by Jang (Jang 1993) in 1993. In fact, ANFIS employs an ANN to optimize the fuzzy logic used in this model (Dehnavi et al. 2015). As a result, it has been shown that ANFIS performs better than the typical fuzzy inference system. As Figure 4 explains, let Q_{ji} be the response of the j^{th} layer, the performance of the ANFIS can be expressed in five steps (Jang 1993):

The first layer has square nodes. Assuming x and y as the input variables, the nodes perform like Equations (5) and (6):

$$Q_{1,i} = \mu F_i(x) \tag{5}$$

$$Q_{1,i} = \mu G_i(y) \tag{6}$$

in which F and G define the linguistic variables and $\mu F_i(x)$ and $\mu G_i(y)$ are the MFs of the corresponding node.

In the second layer, the nodes respond to all input signals as follows:

$$Q_{2,i} = W_i = \mu F_i(x) \mu G_i(y), \quad i = 1, 2 \quad (7)$$

The nodes in Layer 3 aim to normalize the previous outputs and present them as the new ones.

$$Q_{3,i} = \bar{w}_i = \frac{w_i}{w_1 + w_2}, \quad i = 1, 2 \quad (8)$$

In the fourth layer, the nodes with the result parameters of j_i , k_i , and l_i calculate the output as follows:

$$Q_{4,i} = \bar{w}_i f_i = \bar{w}_i (j_i x + k_i y + l_i) \quad (9)$$

Finally, the overall output of the ANFIS is calculated in the fifth layer:

$$Q_{5,i} = \sum \bar{w}_i f_i = \frac{\sum w_i f_i}{\sum w_i}, \quad i = 1, 2 \quad (10)$$

4.3. Metaheuristic techniques

4.3.1. Genetic algorithm

Due to the drawbacks of the typical intelligent models (e.g. the ANFIS and ANN), various natural-inspired metaheuristic algorithms are invented to remedy these shortcomings. The genetic algorithm (GA) is one of these techniques first suggested by Holland (Holland 1975). This algorithm has been widely used for various optimization aims (Jaafari et al. 2019). Figure 5 denotes the flowchart of the GA. Five operators, including the random number generator, fitness evaluation unit, a genetic operator (i.e. for reproduction), crossover operation, and mutation operation, construct the structure of this algorithm. Like other evolutionary algorithms, the GA gets started with creating an initial population (i.e. random strings generated by the random generator). Frequently, binary strings are used in this step which each one of them addresses a possible solution for the defined problem. Next, the evaluation unit evaluates the quality of them by means of a fitness function. The basis of the genetic operators is to transfer the strings into the more fitted sets (i.e. with higher fitness value). The higher the fitness of the strings, the higher the chance for being selected for the next generation. This selection is carried out by the reproduction operator with respect to the “seeded selection” function. The primary duty of the crossover operator is to select the pairs of strings for producing new ones. In this step, a crossover rate is defined to determine the number of the crossover operations that want to cut the original parent strings and change their tails. Also, the mutation operators exist for randomly mutation or reversion of the bits in the strings. All in all, executing the mentioned procedures leads to developing a new generation of solutions (Pham and Karaboga 1991).

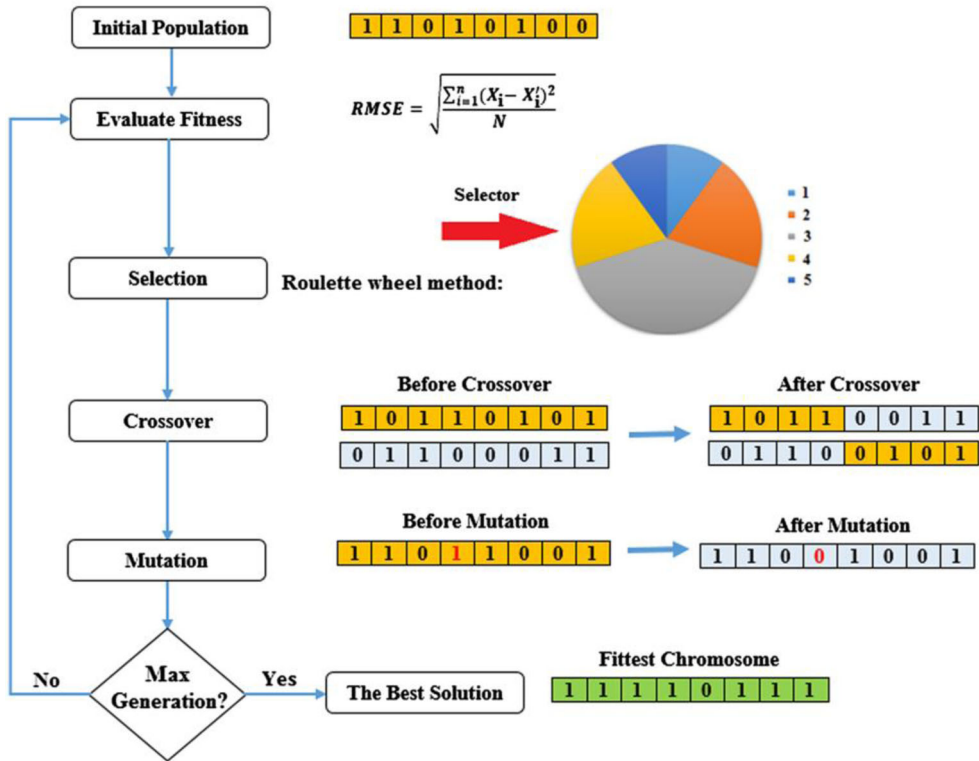


Figure 5. The main flowchart of the genetic algorithm.

4.3.2. Particle swarm optimization

PSO is another powerful search method. Mimicking the foraging behavior of the herds, the idea of the PSO metaheuristic technique was first presented by Kennedy and Eberhart (Kennedy and Eberhart 1995). This technique has been effectively used for optimizing the ANFIS and ANN networks (Nguyen, Moayedi, et al. 2019). Like the GA, some initial relations (called swarm) are randomly produced at the beginning of the PSO. Each possible solution of this algorithm emerges as so-called individuals “particle,” which a random position and velocity are assigned to each one of them. After evaluating the potential of each particle (i.e. through calculating a fitness value), the best solution (i.e. the highest-fitted one) is saved in hyperspace, and the obtained fitness is memorized.

According to the PSO, the defined objective function (i.e. which needs to be minimized for a promising solution) is consecutively measured at the current locations of the particles in the search space. Generally, the particles tend to approach the locations which yield the lowest objective function. The procedure can be summarized as follows (Poli et al. 2007):

1. Generating the initial swarm randomly.
2. loop.
3. Evaluating the goodness of the response of each particle.
4. Regulating the particle’s fitness.

5. Memorizing the elite particle in the vicinity.
6. Computing and updating the velocity and positions of the particle as follows:

$$\vec{x}(t + 1) = \vec{x}(t) + \vec{v}(t + 1) \quad (11)$$

$$\vec{v}(t + 1) = \omega\vec{v}(t) + \phi_1 \text{rand}(0, 1) (\vec{p}(t) - \vec{x}(t)) + \phi_2 \text{rand}(0, 1) (\vec{g}(t) - \vec{x}(t)) \quad (12)$$

in which ϕ_1 and ϕ_2 symbolize the significance of $\vec{p}(t)$ and $\vec{g}(t)$, respectively. Also, the term ω is the inertia weight.

7. Exiting the loop if one of the stopping criteria is met (e.g. the desired fitness or the maximum number of the repetitions).
8. end loop

5. Results and discussion

As stated previously, the main effort of this research is to generate the landslide susceptibility map of the Ardabil province of Iran. To achieve this, two well-known metaheuristic algorithms were coupled with ANFIS to develop the GA-ANFIS and PSO-ANFIS ensembles. In addition, the SI model was also implemented to analyse the risk of landslide occurrence in the proposed area. In this way, the programming software of MATLAB version 14.0 and ArcGIS version 10.2 are used.

5.1. Hybridizing ANFIS using GA and PSO

Specifically speaking, the optimizers are contributed to the problem through fine-tuning the ANFIS MF (Gaussian in this work) parameters assigned to landslide related factors. The adjusted parameters are then used to reconstruct the network. The process is illustrated in [Figure 6](#).

When it comes to artificial intelligence techniques, finding the optimal structure of the used models is overly highlighted. In this study, the complexity of the GA-ANFIS and PSO-ANFIS ensembles are optimized by establishing a trial and error process. In this sense, the mean square error (MSE) index was defined as the cost function of the mentioned networks:

$$MSE = \frac{1}{N} \sum_{i=1}^N (Y_{i \text{ observed}} - Y_{i \text{ predicted}})^2 \quad (13)$$

where N is the number of instances, and $Y_{i \text{ observed}}$, and $Y_{i \text{ predicted}}$ denote the target data and predicted values of landslide susceptibility index, respectively.

Next, ten different structures of both GA-ANFIS and PSO-ANFIS models (i.e. with the population sizes of 50, 100, 150, ..., 500) were tested. The results are presented in [Figures 7](#) – (a) and (b), respectively, for the GA-ANFIS and PSO-ANFIS ensembles. As is seen, the lowest MSE after the 1000 iterations is obtained for the GA-ANFIS (MSE = 0.1162) and PSO-ANFIS (MSE = 0.1200) networks with the population sizes of 250 and 150, respectively. About the optimization speed of these

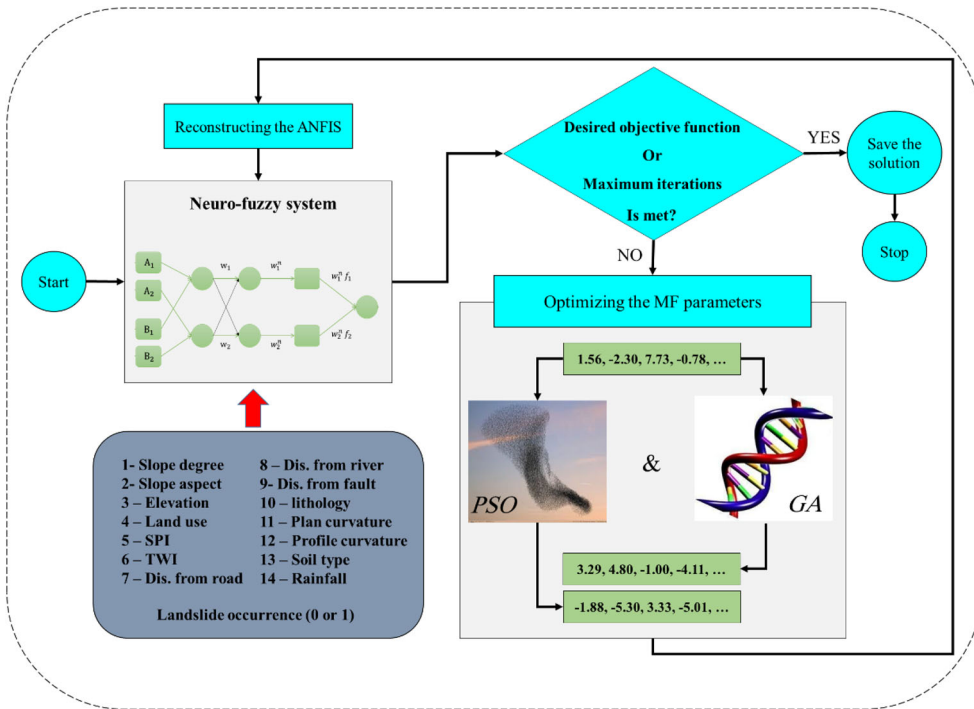
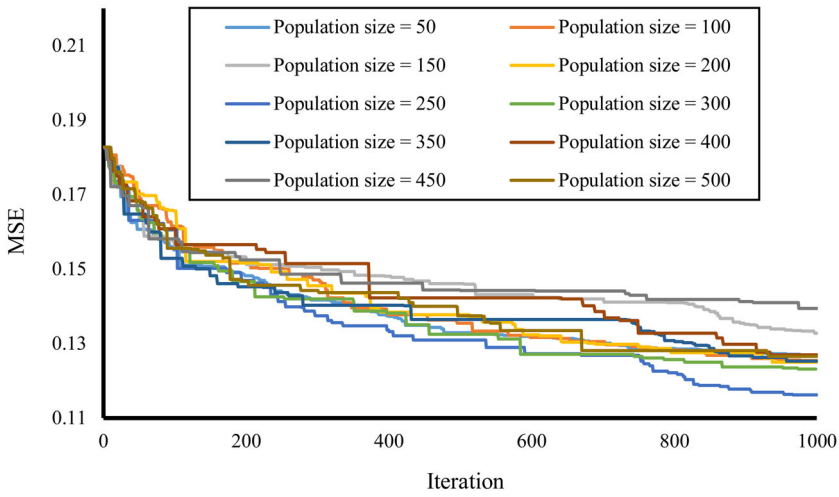


Figure 6. The ANFIS optimization process.

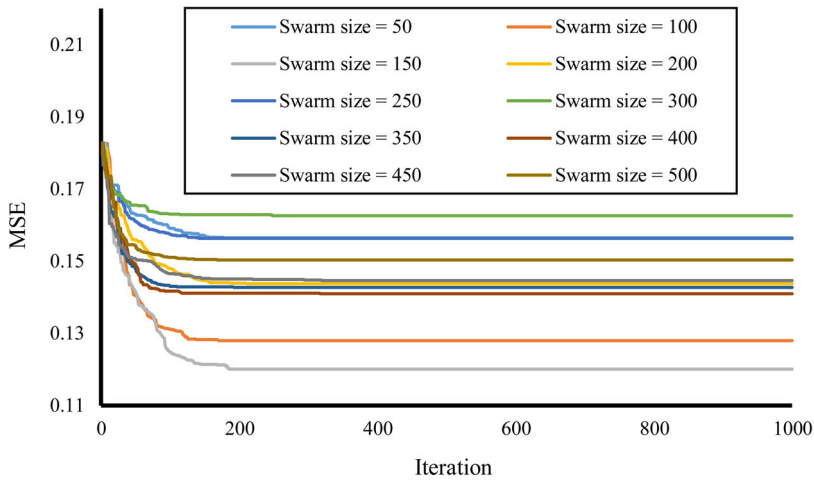
methods, it is obvious that the GA-based fuzzy system has continued decreasing the RMSE until the last try, while the other model has reached the lowest MSE before the 200th repetition.

5.2. Generating the susceptibility maps

In the following, each one of the SI, GA-ANFIS, and PSO-ANFIS was used to estimate the landslide susceptibility values. The resulted values were depicted in the GIS environment to produce the landslide susceptibility maps. Next, each map was classified into five hazard categories of “Very low,” “Low,” “Moderate,” “High,” and “Very high,” with respect to the natural break classification method, which is highly-used in previous studies (Akgun et al. 2012; Jaafari et al. 2014). The resulted landslide susceptibility maps of the Ardabil produced by SI, GA-ANFIS, and PSO-ANFIS evaluative models are shown in Figures 8 – (a-c), respectively. Moreover, the percentage of each susceptibility class was derived for the SI, GA-ANFIS, and PSO-ANFIS models. The results are shown in the form of a bar chart presented in Figures 8 – (d). As the chart illustrates, the most significant distinction between the values refers to the percentage of the areas categorized as safe (i.e. shallow susceptibility) and perilous (i.e. very high susceptibility). More than one-fourth (i.e. 26.93%) of the Ardabil province is detected as hazardous area according to the SI prediction. This is while, the GA-ANFIS and PSO-ANFIS have predicted this value as 8.37% and 12.26%, respectively. In vice versa, the SI has classified only 15% of the area as the relatively safe. These values



(a)



(b)

Figure 7. A population-based sensitivity analysis for the GA-ANFIS and PSO-ANFIS models002E.

obtained as 28.78% and 36.21%, respectively for the GA-ANFIS and PSO-ANFIS predictive tools.

5.3. Accuracy assessment

As mentioned, to evaluate the accuracy of the outputs of the used models, the AUROC index was calculated. To this end, the ROC curve of both training and testing samples were plotted. Figures 9 – (a) and (b) illustrate the generated ROC curves of the training and testing landslides, respectively. According to these diagrams, GA-ANFIS (AUROC = 0.914) achieved the highest AUROC in the training phase, followed by POS-ANFIS (AUROC = 0.910), and SI (AUROC = 0.873) models. This is

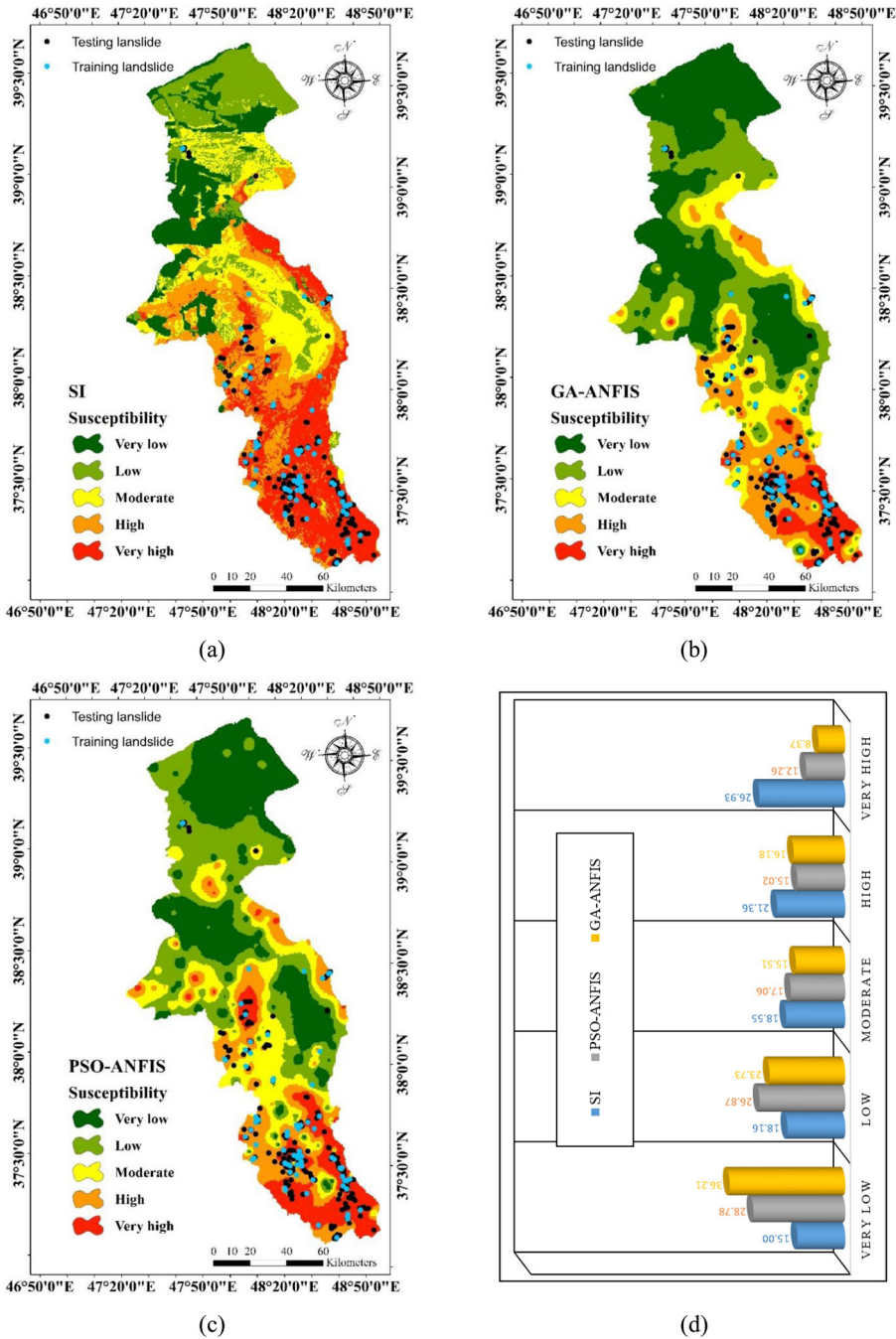


Figure 8: Landslide susceptibility map developed by (a) SI, (b) GA-ANFIS, and (c) PSO-ANFIS models, and (d) column chart showing the percentage of landslide susceptibility classes over the study area. Source: Author

while the SI (AUROC = 0.821) emerged as the most accurate model in the testing phase. After that, the PSO-ANFIS (AUROC = 0.815) showed a more generalization capability compared to the GA-ANFIS (AUROC = 0.773) model.

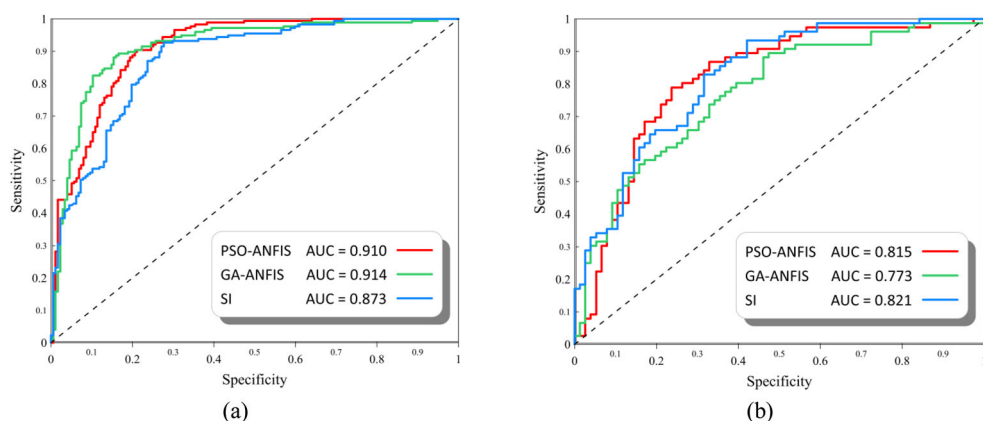


Figure 9. The ROC diagrams plotted for the (a) training and (b) testing data.

In the following, the response of the GA-ANFIS and PSO-ANFIS ensembles is compared with the landslide target values (i.e. 0 and 1) in more detail. To do so, the MSE and mean absolute error (MAE) of the training results were computed. Besides, a graphical comparison between the output and target variables, coupled with the histogram of the calculated errors, are plotted. These charts are shown in Figure 10. Referring to these figures, the calculated MAE and MSE indices support the results obtained from the ROC curves. Accordingly, the training MAE (0.24654 for the GA-ANFIS vs. 0.25654 for the PSO-ANFIS) and MSE (0.11627 vs. 0.12001) denote a higher learning quality of the first ensemble. As for the testing samples, the obtained MAE (0.35335 vs. 0.32032) and MSE (0.21563 vs. 0.17854) show more consistency for the PSO-ANFIS test results.

Lastly, it was aimed to evaluate the accuracy of the results by calculating the percentage of the landslides locate in each susceptibility class. In this manner, the larger the percentage of the located landslides in the perilous areas, the higher the accuracy of the model. The results are depicted in the form of 3D bar charts for both training and testing landslides in Figures 11 – (a) and (b), respectively. As these charts report, the percentage of the landslides is directly proportional to the risk level. In detail, 95.18%, 86.80%, and 97.38% of the training landslides, and 96.42%, 83.89%, and 75.78% of the testing landslides are recognized to be in the hazardous (i.e. high and very high susceptibility classes) regions. It should be noted that the perilous areas of the SI map have contained the highest percentage of both training and testing landslides, and the “very high” susceptibility class of the GA-ANFIS has contained only around 9% of the training slope failures.

This study revealed the competency of metaheuristic-based learning for spatial assessment of landslide, which is a frequent devastating environmental hazard. The ANFIS is a leading notion of machine learning techniques that have been successfully applied to various issues, including groundwater modeling (Chen, Panahi, et al. 2019; Kisi et al. 2019), treatments of natural gas storage (Liu et al. 2020), and forest fire hazard assessment (Jaafari et al. 2019). But there are some drawbacks of this tool for high dimensional problems which (according to the findings of earlier studies) require the assist of metaheuristic techniques for overcoming them. A significant

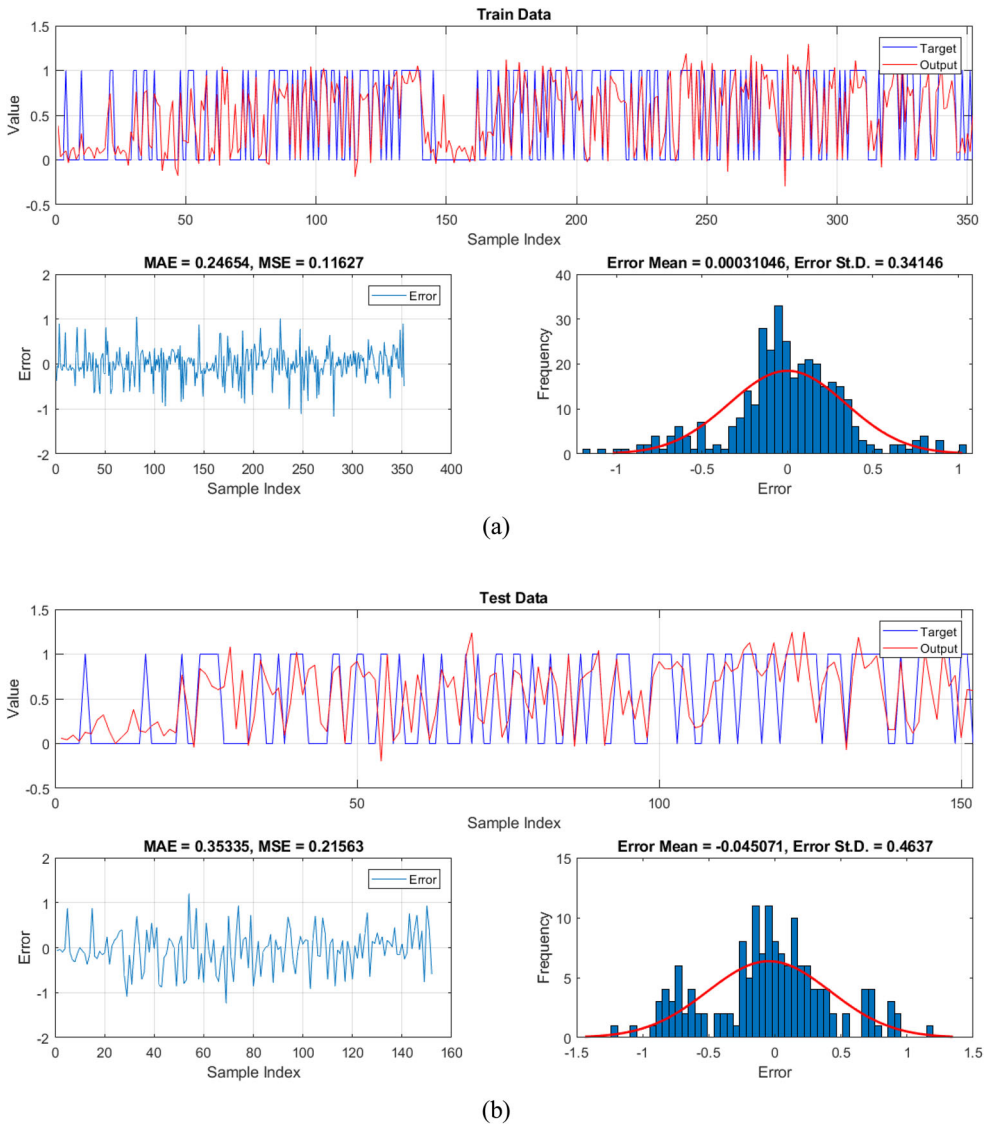
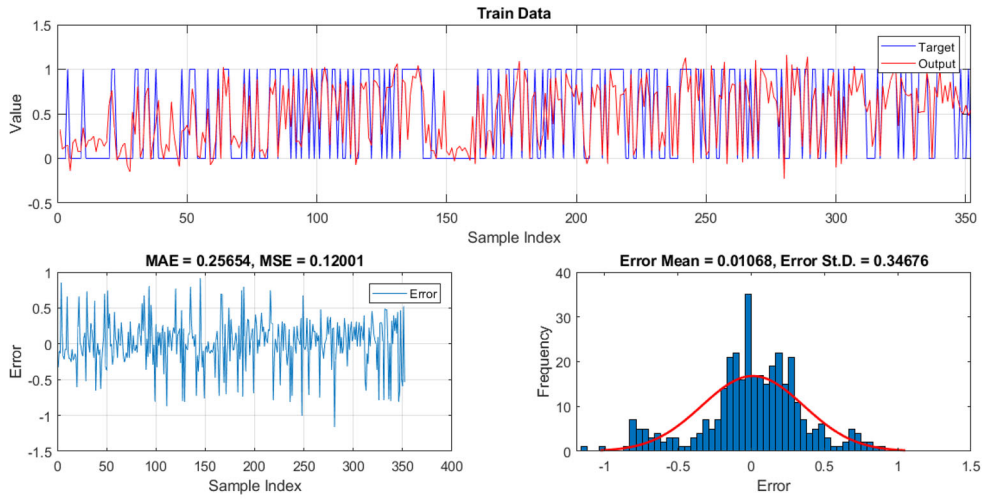
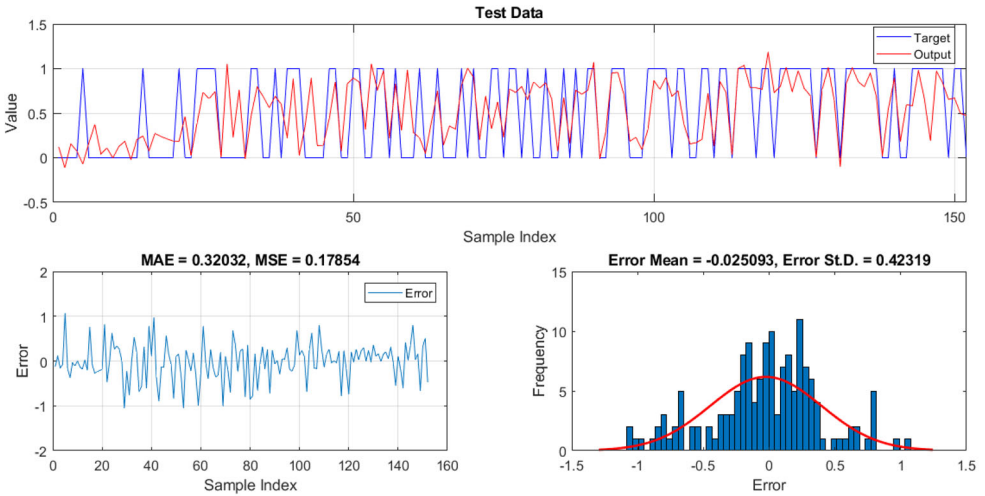


Figure 10. The results obtained for (a and b) GA-ANFIS and (c and d) PSO-ANFIS predictions, respectively, for the training and testing samples.

outcome of the study is the adaptability of this tool with hybrid metaheuristic algorithms of GA and PSO, like Ref. Azad et al. (2018), in which, the authors enhanced the accuracy of ANFIS using GA, ant colony optimization for continuous domains and differential evolution for estimating water quality parameters. In such schemes, the computational parameters of the ANFIS MFs are supposed to be adjusted using stochastic search methods. Considering the number of iterations and the tested complexities (i.e. the population sizes), the optimal solution was automatically derived from $(10 \times 1000 =)$ 10000 possible responses. It reflects an advantage of the optimization techniques that enabled engineers to achieve the most suitable network without implementing time-consuming trial and error processes (Nhu et al. 2019).



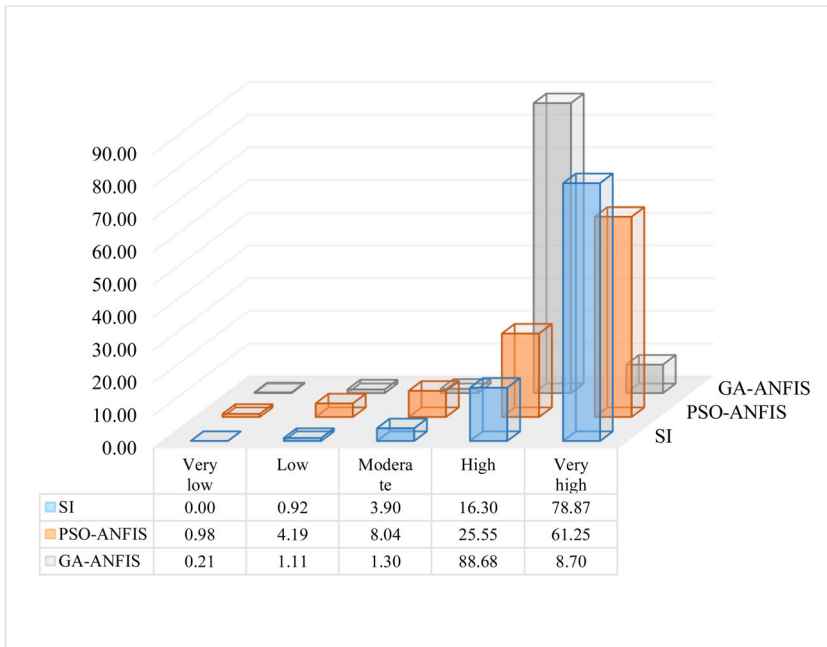
(c)



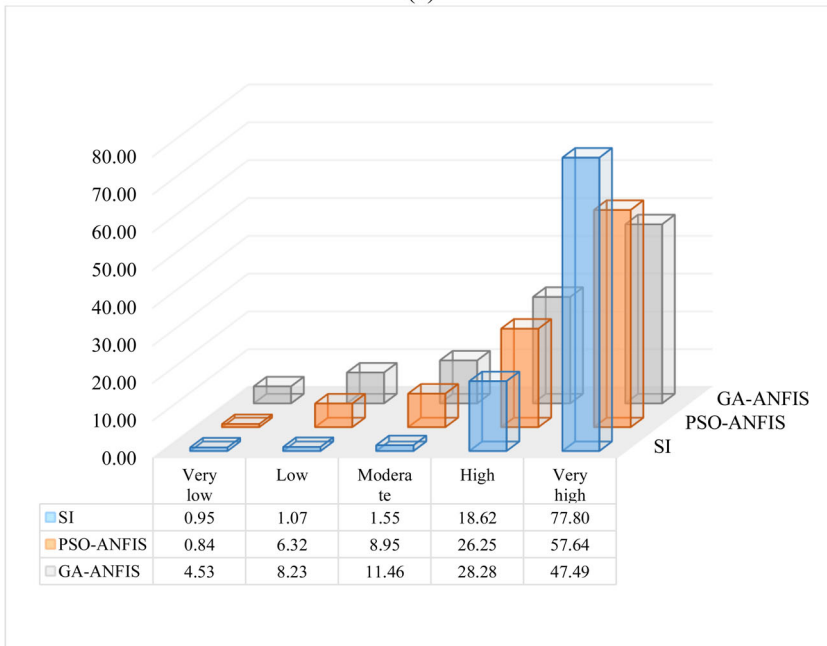
(d)

Figure 10. (Continued).

It was also shown that the PSO performs more accurately than GA in predicting the landside susceptibility for unseen environmental conditions. It indicates the constant optimization method of the PSO (that maintains the suitable solutions of all particles) was more efficient than the discrete method of the GA in which the prior knowledge is replaced with new the information of new generation (Termeh et al. 2018). Regarding higher than 90% and 80% accuracies for inferring and generalizing the landslide patterns, the PSO-ANFIS intelligent model can be a promising option for susceptibility analysis of landslide. Lastly, we believe the generated maps are reliable guides for future planning and decision making over the studied area.



(a)



(b)

Figure 11. The percentage of the (a) training and (b) testing landslides located in each susceptibility classes.

6. Conclusions and remarks

Due to the high significance of landslide susceptibility assessment for alleviating the damages caused by this natural hazard, this study proposes the landslide susceptibility

maps of the Ardabil province of Iran, produced by the SI, GA-ANFIS, and PSO-ANFIS predictive models. The proposed ensembles were designed, and a trial and error process was carried out to achieve the most appropriate complexity of them. It was revealed that the GA-ANFIS with the population sizes = 250 and PSO-ANFIS with the population sizes = 150 yields the lowest values of the objective function. The SI method was executed, and the landslide susceptibility maps were developed in the GIS environment. The AUROC index was used to evaluate the accuracy of the results. The outcomes of this research are summarized as follows:

- Based on the obtained AUROCs in training (0.873, 0.914, and 0.910, respectively for the SI, GA-ANFIS, and PSO-ANFIS) and testing (0.821, 0.773, and 0.815) phases, all three predictive models showed a gratifying analysis of the landslide occurrence risk.
- The GA-ANFIS and SI present the best performance in the training and testing phases, respectively. While the lowest training and testing accuracy of the prediction is obtained respectively for the SI and GA-ANFIS models. At the same time, the PSO-ANFIS remained the second accurate model in both phases.
- Comparing the efficacy of the intelligent models, the calculated training MAE (0.24654 for the GA-ANFIS vs. 0.25654 for the PSO-ANFIS) and training MSE (0.11627 vs. 0.12001) as well as the testing MAE (0.35335 vs. 0.32032) and testing MSE (0.21563 vs. 0.17854) show that the GA-ANFIS has a better approximation in the training phase.
- Approximately 48%, 25%, and 27% of the Ardabil province are stratified as the landslide-prone regions, respectively, by the SI, GA-ANFIS, and PSO-ANFIS models.
- Also, around 95%, 87%, and 97% of the training landslides, and 96%, 84%, and 76% of the testing landslides are located in the landslide perilous areas.

Disclosure statement

No potential conflict of interest was reported by the authors.

ORCID

Hossein Moayedi  <http://orcid.org/0000-0002-5625-1437>

References

- Ahmadlou M, Karimi M, Alizadeh S, Shirzadi A, Parvinnejhad D, Shahabi H, Panahi M. 2018. Flood susceptibility assessment using integration of adaptive network-based fuzzy inference system (ANFIS) and biogeography-based optimization (BBO) and BAT algorithms (BA). *Geocarto Int.* 1–21.
- Akgun A, Sezer EA, Nefeslioglu HA, Gokceoglu C, Pradhan B. 2012. An easy-to-use MATLAB program (MamLand) for the assessment of landslide susceptibility using a Mamdani fuzzy algorithm. *Comput Geosci.* 38:23–34.
- Akkurt S, Ozdemir S, Tayfur G, Akyol B. 2003. The use of GA-ANNs in the modelling of compressive strength of cement mortar. *Cem Concr Res.* 33(7):973–979.

- Azad A, Karami H, Farzin S, Saedian A, Kashi H, Sayyahi F. 2018. Prediction of water quality parameters using ANFIS optimized by intelligence algorithms (case study: Gorganrood River). *KSCE J Civ Eng.* 22(7):2206–2213.
- Azad A, Manoochehri M, Kashi H, Farzin S, Karami H, Nourani V, Shiri J. 2019. Comparative evaluation of intelligent algorithms to improve adaptive neuro-fuzzy inference system performance in precipitation modelling. *J Hydrol.* 571:214–224.
- Bagheri V, Uromeihy A, Aghda S. 2018. Evaluation of ANFIS and LR models for seismic rock-falls' susceptibility mapping: a case study of Firooz Abad-Kojour, Iran, Earthquake (2004). *Environ Earth Sci.* 77:800.
- Cevik E, Topal T. 2003. GIS-based landslide susceptibility mapping for a problematic segment of the natural gas pipeline, Hendek (Turkey). *Environ Geol.* 44(8):949–962.
- Chen J, Lu D, Liu W, Fan J, Jiang D, Yi L, Kang Y. 2020. Stability study and optimization design of small-spacing two-well (SSTW) salt caverns for natural gas storages. *J Energy Storag.* 27:101131. doi:10.1016/j.est.2019.101131
- Chen W, Panahi M, Khosravi K, Pourghasemi HR, Rezaie F, Parvinnezhad D. 2019. Spatial prediction of groundwater potentiality using ANFIS ensemble with teaching-learning-based and biogeography-based optimization. *J Hydrol.* 572:435–448.
- Chen W, Panahi M, Pourghasemi HR. 2017. Performance evaluation of GIS-based new ensemble data mining techniques of adaptive neuro-fuzzy inference system (ANFIS) with genetic algorithm (GA), differential evolution (DE), and particle swarm optimization (PSO) for landslide spatial modelling. *Catena.* 157:310–324.
- Chen W, Pourghasemi HR, Panahi M, Kornejady A, Wang J, Xie X, Cao S. 2017. Spatial prediction of landslide susceptibility using an adaptive neuro-fuzzy inference system combined with frequency ratio, generalized additive model, and support vector machine techniques. *Geomorphology.* 297:69–85.
- Chen W, Yan X, Zhao Z, Hong H, Bui DT, Pradhan B. 2019. Spatial prediction of landslide susceptibility using data mining-based kernel logistic regression, naive Bayes and RBFNetwork models for the Long County area (China). *Bull Eng Geol Environ.* 78(1): 247–266.
- Chen W, Zhang S, Li R, Shahabi H. 2018. Performance evaluation of the GIS-based data mining techniques of best-first decision tree, random forest, and naïve Bayes tree for landslide susceptibility modeling. *Sci Total Environ.* 644:1006–1018.
- Dehnavi A, Aghdam IN, Pradhan B, Varzandeh M. 2015. A new hybrid model using step-wise weight assessment ratio analysis (SWARA) technique and adaptive neuro-fuzzy inference system (ANFIS) for regional landslide hazard assessment in Iran. *Catena.* 135:122–148.
- Demir G, Aytekin M, Akgun A. 2015. Landslide susceptibility mapping by frequency ratio and logistic regression methods: an example from Niksar-Resadiye (Tokat, Turkey). *Arab J Geosci.* 8(3):1801–1812.
- Ercanoglu M, Gokceoglu C. 2004. Use of fuzzy relations to produce landslide susceptibility map of a landslide prone area (West Black Sea Region, Turkey). *Eng Geol.* 75(3-4):229–250.
- Fan J, Jiang D, Liu W, Wu F, Chen J, Daemen J. 2019. Discontinuous fatigue of salt rock with low-stress intervals. *Int J Rock Mech Min Sci.* 115:77–86. doi:10.1016/j.ijrmmms.2019.01.013
- Gao W, Dimitrov D, Abdo H. 2018. Tight independent set neighborhood union condition for fractional critical deleted graphs and ID deleted graphs. *Discrete Contin Dyn Syst.* 12: 711–721.
- Gao W, Guirao JLG, Abdel-Aty M, Xi W. 2019. An independent set degree condition for fractional critical deleted graphs. *Discrete Contin Dyn Syst.* 12:877–886.
- Gao W, Guirao JLG, Basavanagoud B, Wu J. 2018. Partial multi-dividing ontology learning algorithm. *Inf Sci.* 467:35–58.
- Gao W, Wang W, Dimitrov D, Wang Y. 2018. Nano properties analysis via fourth multiplicative ABC indicator calculating. *Arab J Chem.* 11(6):793–801.
- Gao W, Wu H, Siddiqui MK, Baig AQ. 2018. Study of biological networks using graph theory. *Saudi J Biol Sci.* 25(6):1212–1219.

- He Q, Shahabi H, Shirzadi A, Li S, Chen W, Wang N, Chai H, Bian H, Ma J, Chen Y. 2019. Landslide spatial modelling using novel bivariate statistical based Naïve Bayes, RBF Classifier, and RBF Network machine learning algorithms. *Sci Total Environ.*663:1–15.
- Holland JH. 1975. Adaptation in natural and artificial systems: an introductory analysis with applications to biology, control, and artificial intelligence. In: University of Michigan press Ann Arbor.
- Hong H, Miao Y, Liu J, Zhu AX. 2019. Exploring the effects of the design and quantity of absence data on the performance of random forest-based landslide susceptibility mapping. *Catena.* 2019/05/01/176:45–64.
- Hong H, Panahi M, Shirzadi A, Ma T, Liu J, Zhu A-X, Chen W, Kougiaris I, Kazakis N. 2018. Flood susceptibility assessment in Hengfeng area coupling adaptive neuro-fuzzy inference system with genetic algorithm and differential evolution. *Sci Total Environ.* 621:1124–1141.
- Jaafari A, Najafi A, Pourghasemi H, Rezaeiian J, Sattarian A. 2014. GIS-based frequency ratio and index of entropy models for landslide susceptibility assessment in the Caspian forest, northern Iran. *Int J Environ Sci Technol.* 11(4):909–926.
- Jaafari A, Zenner EK, Panahi M, Shahabi H. 2019. Hybrid artificial intelligence models based on a neuro-fuzzy system and metaheuristic optimization algorithms for spatial prediction of wildfire probability. *Agric Forest Meteorol.* 266:198–207.
- Jang J-S. 1993. ANFIS: adaptive-network-based fuzzy inference system. *IEEE Trans Syst ManCybern.* 23(3):665–685.
- Kaur H, Gupta S, Parkash S, Thapa R, Gupta A, Khanal G. 2019. Evaluation of landslide susceptibility in a hill city of Sikkim Himalaya with the perspective of hybrid modelling techniques. *Annals of GIS.* 25:113–132.
- Kennedy J, Eberhart R. 1995. Particle swarm optimization. Proceedings of the Proceedings of ICNN'95 - International Conference on Neural Networks; 27 Nov.-1 Dec. 1995.
- Kisi O, Azad A, Kashi H, Saeedian A, Hashemi SAA, Ghorbani S. 2019. Modeling groundwater quality parameters using hybrid neuro-fuzzy methods. *Water Resour Manage.* 33(2): 847–861.
- Kisi O, Keshavarzi A, Shiri J, Zounemat-Kermani M, Omran E-SE. 2017. Groundwater quality modeling using neuro-particle swarm optimization and neuro-differential evolution techniques. *Hydrol Res.* 48(6):1508–1519.
- Kornejady A, Pourghasemi HR. 2019. Producing a spatially focused landslide susceptibility map using an ensemble of Shannon's entropy and fractal dimension (Case Study: Ziarat Watershed, Iran). In: *Spatial Modeling in GIS and R for Earth and Environmental Sciences.* Elsevier. Oxford. p. 689–732.
- Lee S, Hong S-M, Jung H-S. 2017. A support vector machine for landslide susceptibility mapping in Gangwon Province, Korea. *Sustainability.* 9(1):48.
- Liu W, Zhang Z, Chen J, Fan J, Jiang D, Jjk D, Li Y. 2020. Physical simulation of construction and control of two butted-well horizontal cavern energy storage using large molded rock salt specimens. *Energy.* 185:682–694. Doi: [10.1016/j.energy.2019.07.014](https://doi.org/10.1016/j.energy.2019.07.014)
- Malik A, Kumar A, Kisi O, Shiri J. 2019. Evaluating the performance of four different heuristic approaches with Gamma test for daily suspended sediment concentration modeling. *Environ Sci Pollut Res.* 26:1–18.
- Moayedi H, Mehrabi M, Mosallanezhad M, Rashid ASA, Pradhan B. 2018. Modification of landslide susceptibility mapping using optimized PSO-ANN technique. *Eng Comput.* 35(3): 967–984.
- Moore ID, Grayson R, Ladson A. 1991. Digital terrain modelling: a review of hydrological, geomorphological, and biological applications. *Hydrol Process.* 5(1):3–30.
- Nguyen H, Mehrabi M, Kalantar B, Moayedi H, Abdullahi MM. 2019. Potential of hybrid evolutionary approaches for assessment of geo-hazard landslide susceptibility mapping. *Geomat Nat Haz Risk.* 10(1):1667–1693.
- Nguyen H, Moayedi H, Foong LK, Al Najjar HAH, Jusoh WAW, Rashid ASA, Jamali J. 2019. Optimizing ANN models with PSO for predicting short building seismic response. *Eng Comput.* 1–15. doi:[10.1007/s00366-019-00733-0](https://doi.org/10.1007/s00366-019-00733-0)

- Nguyen V, Pham B, Vu B, Prakash I, Jha S, Shahabi H, Shirzadi A, Ba D, Kumar R, Chatterjee J, et al. 2019. Hybrid machine learning approaches for landslide susceptibility modeling. *Forests*. 10(2):157.
- Nhu V-H, Hoang N-D, Duong V-B, Vu H-D, Bui DT. 2019. A hybrid computational intelligence approach for predicting soil shear strength for urban housing construction: a case study at Vinhomes Imperia project, Hai Phong city (Vietnam). *Eng Comput*. 1–14. doi:10.1007/s00366-019-00718-z
- Oh H-J, Kim Y-S, Choi J-K, Park E, Lee S. 2011. GIS mapping of regional probabilistic groundwater potential in the area of Pohang City, Korea. *J Hydrol*. 399(3-4):158–172.
- Oh H-J, Pradhan B. 2011. Application of a neuro-fuzzy model to landslide-susceptibility mapping for shallow landslides in a tropical hilly area. *Comput Geosci*. 37:1264–1276.
- Pham BT, Prakash I, Chen W, Ly H-B, Ho LS, Omidvar E, Tran VP, Bui DT. 2019. A novel intelligence approach of a sequential minimal optimization-based support vector machine for landslide susceptibility mapping. *Sustainability*. 11:6323.
- Pham B T, Prakash I, Singh S K, Shirzadi A, Shahabi H, Tran T-T-T, Bui D T. 2019. Landslide susceptibility modeling using Reduced Error Pruning Trees and different ensemble techniques: hybrid machine learning approaches. *Catena*. 175:203–218.
- Pham D, Karaboga D. 1991. Optimum design of fuzzy logic controllers using genetic algorithms. *J Syst Eng*. 1:114–118.
- Poli R, Kennedy J, Blackwell T. 2007. Particle swarm optimization. *Swarm Intell*. 1(1):33–57.
- Polykretis C, Chalkias C, Ferentinou M. 2017. Adaptive neuro-fuzzy inference system (ANFIS) modeling for landslide susceptibility assessment in a Mediterranean hilly area. *Bull Eng Geol Environ*. 78(2):1173–1187.
- Pourghasemi H, Moradi H, Aghda SF. 2013. Landslide susceptibility mapping by binary logistic regression, analytical hierarchy process, and statistical index models and assessment of their performances. *Nat Hazards*. 69(1):749–779.
- Pourghasemi HR, Mohammady M, Pradhan B. 2012. Landslide susceptibility mapping using index of entropy and conditional probability models in GIS: Safarood Basin, Iran. *Catena*. 97:71–84.
- Pourghasemi HR, Pradhan B, Gokceoglu C. 2012. Application of fuzzy logic and analytical hierarchy process (AHP) to landslide susceptibility mapping at Haraz watershed, Iran. *Nat Hazards*. 63(2):965–996.
- Qiao W, Huang K, Azimi M, Han S. 2019. A novel hybrid prediction model for hourly gas consumption in supply side based on improved whale optimization algorithm and relevance vector machine. *IEEE Access*. 7:88218–88230. doi:10.1109/ACCESS.2019.2918156
- Qiao W, Lu H, Zhou G, Azimi M, Yang Q, Tian W. 2020. A hybrid algorithm for carbon dioxide emissions forecasting based on improved lion swarm optimizer. *J Clean Prod*. 244: 118612. doi:10.1016/j.jclepro.2019.118612
- Qiao W, Tian W, Tian Y, Yang Q, Wang Y, Zhang J. 2019. The Forecasting of PM2.5 Using a Hybrid Model Based on Wavelet Transform and an Improved Deep Learning Algorithm. *IEEE Access*. 7:142814–142825. doi:10.1109/ACCESS.2019.2944755.
- Qiao W, Yang Z. 2019a. Forecast the electricity price of U.S. using a wavelet transform-based hybrid model. *Energy*. 193: 16704. doi:10.1016/j.energy.2019.116704
- Qiao W, Yang Z. 2019b. Modified dolphin swarm algorithm based on chaotic maps for solving high-dimensional function optimization problems. *IEEE Access*. 7:110472–110486. doi:10.1109/ACCESS.2019.2931910
- Qiao W, Yang Z. 2019c. Solving large-scale function optimization problem by using a new metaheuristic algorithm based on quantum dolphin swarm algorithm. *IEEE Access*. 7: 138972–138989. doi:10.1109/ACCESS.2019.2942169
- Qiao W, Yang Z. 2020. An improved dolphin swarm algorithm based on Kernel Fuzzy C-means in the application of solving the optimal problems of large-scale function. *IEEE Access*. 8:2073–2089. 09 December 2019. doi:10.1109/ACCESS.2019.2958456

- Qiao W, Yang Z, Kang Z, Pan Z. 2020. Short-term natural gas consumption prediction based on Volterra adaptive filter and improved whale optimization algorithm. *Eng Appl Artif Intell.* 87:103323. [10.1016/j.engappai.2019.103323](https://doi.org/10.1016/j.engappai.2019.103323)
- Shoaei Z, Ghayoumian J. 1998. The largest debris flow in the world, Seimareh Landslide, Western Iran. In: *Environmental Forest Science*. Springer. Dordrecht. p. 553–561.
- Termeh SVR, Kornejady A, Pourghasemi HR, Keesstra S. 2018. Flood susceptibility mapping using novel ensembles of adaptive neuro fuzzy inference system and metaheuristic algorithms. *Sci Total Environ.* 615:438–451.
- Tien Bui D, Pham BT, Nguyen QP, Hoang N-D. 2016. Spatial prediction of rainfall-induced shallow landslides using hybrid integration approach of Least-Squares Support Vector Machines and differential evolution optimization: a case study in Central Vietnam. *Int J Dig Earth.* 9(11):1077–1097.
- Vakhshoori V, Zare M. 2016. Landslide susceptibility mapping by comparing weight of evidence, fuzzy logic, and frequency ratio methods. *Geo Nat Haz Risk.* 7(5):1731–1752.
- Van Westen C. 1997a. Statistical landslide hazard analysis. *ILWIS.* 2:73–84.
- van Westen C. 1997b. Statistical landslide hazard analysis. *ILWIS 2.1 for windows application* Gui de. Enshede. The Netherlands: ITC Publication, p. 73–84.
- Varnes D, Radbruch-Hall D. 1976. Landslides cause and effect. *Bull Int Assoc Eng Geol.* 13: 205–216.
- Wang Q, Li W, Chen W, Bai H. 2015. GIS-based assessment of landslide susceptibility using certainty factor and index of entropy models for the Qianyang County of Baoji city, China. *J Earth Syst Sci.* 124(7):1399–1415.
- Weibiao Q. 2019. Differential Scanning Calorimetry and Electrochemical Tests for the Analysis of Delamination of 3PE Coatings. *Int J Electrochem Sci.* :7389–7400. doi:[10.20964/2019.08.05](https://doi.org/10.20964/2019.08.05).
- Xi W, Li G, Moayedi H, Nguyen H. 2019. A particle-based optimization of artificial neural network for earthquake-induced landslide assessment in Ludian county, China. *Geo Nat Haz Risk.* 10(1):1750–1771.
- Yang J, Song C, Yang Y, Xu C, Guo F, Xie L. 2019. New method for landslide susceptibility mapping supported by spatial logistic regression and GeoDetector: a case study of Duwen Highway Basin, Sichuan Province, China. *Geomorphology.* 324:62–71.
- Liu W, Zhang ZX, Fan JY, Jiang DY, Daemen JJK. 2020. Research on the stability and treatments of natural gas storage caverns with different shapes in bedded salt rocks. *IEEE Access.* 8:000507, doi:[10.1109/ACCESS.2020.2967078](https://doi.org/10.1109/ACCESS.2020.2967078).
- Yesilnacar EK. 2005. The application of computational intelligence to landslide susceptibility mapping in Turkey: University of Melbourne, Department, 200.
- Youssef AM, Pradhan B, Jebur MN, El-Harbi HM. 2015. Landslide susceptibility mapping using ensemble bivariate and multivariate statistical models in Fayfa area, Saudi Arabia. *Environ Earth Sci.* 73(7):3745–3761. Apr
- Zhang Z, Jiang D, Liu W, Chen J, Li E, Fan J, Xie K. 2019. Study on the mechanism of roof collapse and leakage of horizontal cavern in thinly bedded salt rocks. *Environ Earth Sci.* 78(10):292. <https://doi.org/10.1007/s12665-019-8292-2>
- Zhou Moayedi H, Bahiraei M, Lyu Z. 2020. Employing artificial bee colony and particle swarm techniques for optimizing a neural network in prediction of heating and cooling loads of residential buildings. *Journal of Cleaner production* 254, doi:[10.1016/j.jclepro.2020.120082](https://doi.org/10.1016/j.jclepro.2020.120082)